APPLIED SCIENCES AND ENGINEERING

Biosensing near the neutrality point of graphene

Wangyang Fu,[1,2]* Lingyan Feng,[1,3] Gregory Panaitov,[1] Dmitry Kireev,[1] Dirk Mayer,[1] Andreas Offenhäusser,[1] Hans-Joachim Krause[1]

Over the past decade, the richness of electronic properties of graphene has attracted enormous interest for electrically detecting chemical and biological species using this two-dimensional material. However, the creation of practical graphene electronic sensors greatly depends on our ability to understand and maintain a low level of electronic noise, the fundamental reason limiting the sensor resolution. Conventionally, to reach the largest sensing response, graphene transistors are operated at the point of maximum transconductance, where 1/*f* noise is found to be unfavorably high and poses a major limitation in any attempt to further improve the device sensitivity. We show that operating a graphene transistor in an ambipolar mode near its neutrality point can markedly reduce the 1/*f* noise in graphene. Remarkably, our data reveal that this reduction in the electronic noise is achieved with uncompromised sensing response of the graphene chips and thus significantly improving the signal-to-noise ratio—compared to that of a conventionally operated graphene transistor for conductance measurement. As a proof-of-concept demonstration of the usage of the aforementioned new sensing scheme to a broader range of biochemical sensing applications, we selected an HIV-related DNA hybridization as the test bed and achieved detections at picomolar concentrations.

INTRODUCTION

The concept of an ion-sensitive field-effect transistor (ISFET) (*1*, *2*) enables label-free detection of charged molecules on a small footprint upon its binding at the sensor surface, because it modulates the electrical current in the semiconductor channel due to field effect. Recent research trends now offer new opportunities for developing the modern version of a classical ISFET using graphene (and other two-dimensional materials) (*3*–*11*), with demonstrated greater sensitivity than traditional bioassays (*12*). Conventionally, the highest sensing response is reached when the graphene ISFET (GISFET or GFET) is operated at its maximum transconductance, which shows the largest change in the transistor current induced by a small change in the gate voltage. However, at the point of maximum transconductance, the electronic noise is found to be unfavorably large and therefore poses a major limitation to achieve next-generation graphene biochemical sensors with ever-demanding sensitivity (*13*–*15*).

Generally, the ubiquitous 1/*f* noise, whose power spectral density (PSD) inversely depends on the frequency *f*, dominates the noise spectrum of GFETs and determines its detection resolution at biologically relevant low frequencies (≲1000 Hz) (*13*). Earlier studies also determined that, for graphene supported on a SiO_2/Si substrate, the background electrical noise is at minimum near the neutrality point of graphene where the electron density of states is lowest (*16*). In previous studies of graphene sensors in Hall geometry, biasing at this low-noise neutrality point can be favorably designed into the devices with the steepest sensing response in Hall resistivity (*17*, *18*). Unfortunately, these works require an elaborate magnet setup, which is not suitable for integration and portable application. Here, we report an example of graphene chips operated near the low-noise neutrality point in simple transistor geometry (Fig. 1, A and B), without compromising any prospects of a label-free and portable graphene electronic sensor.

[1]Institute of Complex Systems Bioelectronics (ICS-8), Forschungszentrum Jülich, Jülich 52425, Germany. [2]Leiden Institute of Chemistry, Faculty of Science, Leiden University, Einsteinweg 55, 2333CC Leiden, Netherlands. [3]Materials Genome Institute, Shanghai University, Shanghai 200444, China.
*Corresponding author. Email: fwy99@mails.tsinghua.edu.cn

RESULTS AND DISCUSSION

Device preparation: In situ electrochemical cleaning for graphene surface refreshment

We investigated altogether 16 GFET devices prepared by transfer of chemical vapor deposition (CVD) graphene on three different substrates (7 devices on SiO_2/Si, 4 devices on Si_3N_4/SiO_2/Si, and 5 devices on sapphire; see Materials and Methods). Figure 1C shows the scheme of a conventional electrolyte-gated GFET. In Fig. 1D, the transfer curve in gray depicts a typical measured sheet conductance *G* of graphene plotted against the liquid-gate voltage V_{ref} (defined via an Ag/AgCl reference electrode) for an as-fabricated device on a SiO_2/Si substrate (GFET-I). Despite the fact that we treated the SiO_2 with hexamethyldisilazane (HMDS) (*19*) (before graphene transfer) to effectively shield the graphene from trapped charges on the SiO_2 surface, it was common that we observed (Fig. 1D, gray curve) multiple neutrality points (at V_{NP} = −0.11, 0.11, and 0.39 V) and relatively large hysteresis (~50 to 100 mV). These poor device performances against liquid-gate voltage sweeping suggest significant charged trap states at the graphene/electrolyte interface, an indicator of the presence of a large amount of surface contaminants (even though all the devices were baked at ~200°C and thoroughly rinsed in isopropanol; see Materials and Methods) (*20*). To restore highly reliable device characteristics before measurement, the graphene transistor is subjected to an in situ electrochemical cleaning that rapidly removes any surface contaminants from graphene (see Materials and Methods) (*21*–*24*). This electrochemical cleaning technique yields consecutively recovered transfer curves of the GFET-I as shown in Fig. 1D (upper panel, sheet conductance mapping), suggesting a surface refreshment of graphene. Every consecutive cleaning cycle decreases the hysteresis and removes the spurious neutrality points observed at gate voltages of −0.11 and 0.39 V. After 10 cycles of refreshment (red line, Fig. 1D), the $G(V_{ref})$ curve of the GFET-I became completely stable, and we were able to eliminate both the initial hysteresis and the spurious neutrality points observed at V_{ref} = −0.11 and 0.39 V. Further cycling at an operational window of (−0.4 V, 0.6 V) results neither in any shift of the neutrality point nor in any change of the GFETs' conductance. Using an interface capacitance of ~2 μF/cm^2 (*7*), we estimate the field-effect mobility of this electrolyte-gated GFET-I to be ~1100 cm^2/Vs for both hole and electron carriers. This

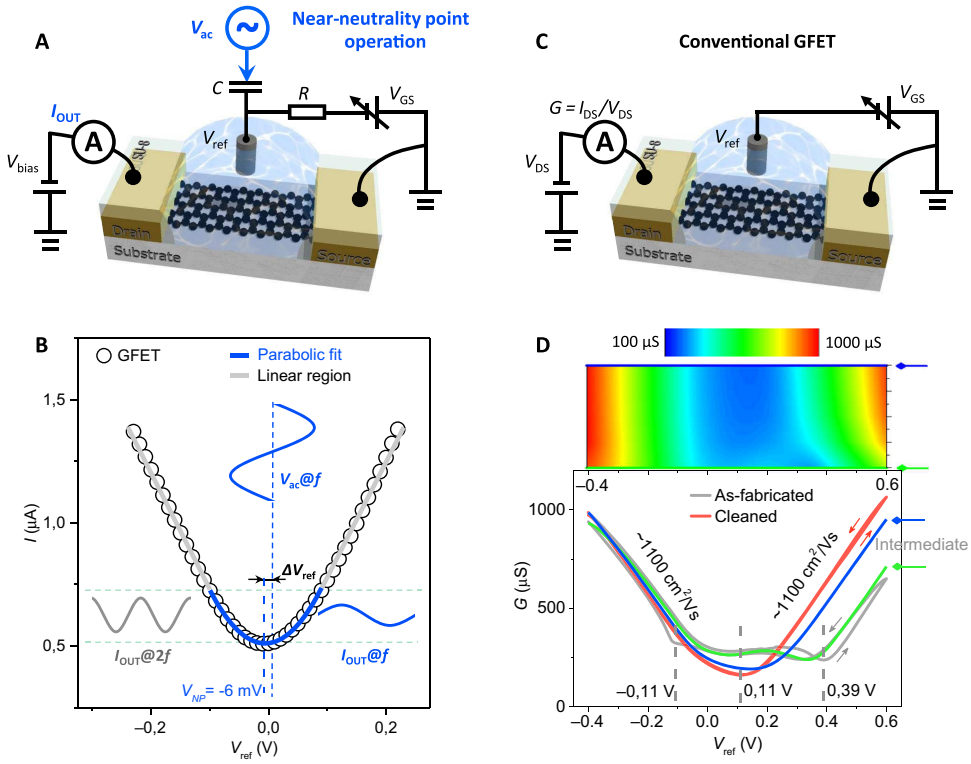

Fig. 1. Near–neutrality point operation and conventional GFET. (**A**) Schematic presentation of near–neutrality point operation of an electrolyte-gated GFET device. (**B**) The transfer curve $I(V_{ref})$ of the GFET-II (black circles, after electrochemical cleaning) and the corresponding parabolic fitting (blue line) around the neutrality point and the linear fit (gray lines) away from the neutrality point. The working principle of the electrolyte-gated GFET operated near the neutrality point is also illustrated in the inset diagram: The output current contains both the second harmonic component $0.5a_0A_{ac}^2 \cos 4\pi ft$ (I_{OUT} at frequency $2f$) and the fundamental component (I_{OUT} at frequency f) $2a_0A_{ac}\Delta V_{ref} \sin 2\pi ft$. All recorded in 1 mM PBS buffer solution. (**C**) Schematic presentation of a conventional electrolyte-gated GFET device. (**D**) Upper panel: Sheet conductance mapping of the GFET-I during electrochemical cleaning cycles with an operational window of V_{ref} = (−0.4 V, 0.6 V). Lower panel: $G(V_{ref})$ curves of the GFET-I before cleaning (gray line), during the first (green line and arrow) and the fifth (blue line and arrow) cleaning cycle, and after 10 times continuous cleaning cycles (red line), which start to show a rather symmetric ambipolar behavior with field-effect mobilities of ~1100 cm^2/Vs for both hole and electron carriers.

mobility number is in good agreement with the field-effect mobility of ~1000 to 1500 cm^2/Vs that we obtained using a Si back gate before the electrochemical surface refreshment and liquid gating, indicating that the underlying Si substrate plays an important role in determining the electrical properties of our GFET devices (*11*).

Graphene transistors operated near the neutrality point with minimum 1/*f* noise

Owing to the lack of an intrinsic band gap (*25*, *26*), the GFETs present typical ambipolar transfer characteristics without an off-state (for example, Fig. 1D; red line). The charge carriers in the graphene channel can be continuously tuned from holes to electrons when sweeping the liquid-gate voltage from negative to positive. At the transition point (0.11 V), which is the so-called charge neutrality point with nearly equal electron and hole densities, the graphene conductance G reaches its minimum value. As a procedure routinely used in many studies, the gate voltage shifts of the $G(V_{ref})$ curves are deduced upon addition of analytes to evaluate the sensing response of a GFET device. However, this procedure cannot be adopted at the neutrality point (where the 1/*f* noise in graphene is optimal) because the transconductance and thus its related sensing response are (close to) zero at this region. Alternatively, here we report an elegant and simple approach permitting low-noise operation near the neutrality point of graphene by harvesting its unique ambipolar behavior: We apply a sine wave to cycle the gate voltage of an electrolyte-gated GFET (GFET-II) around its neutrality point and to monitor the output current in a common-source configuration. As illustrated in Fig. 1A, an ac drive voltage, V_{ac}, with a typical amplitude of 70.7 mV (ranging from 14.1 to 282.8 mV) and a frequency f of 77.77 Hz (ranging from 9.111 to 2.161 kHz), was provided by an SR830 lock-in amplifier (Stanford Research Systems) and delivered to the liquid gate of the GFET. The dc bias drain-source voltage V_{bias} and dc liquid-gate voltage $V_{GS} = V_{NP} + \Delta V_{ref}$ were maintained using homemade battery-based voltage sources, and the rectified output drain current was monitored using the lock-in amplifier.

The nonlinearity of the symmetric $I(V_{ref})$ curve (black circles, Fig. 1B) near the neutrality point plays a key role in the applications. As shown by the fitted blue line (Fig. 1B), we can approximate the $I(V_{ref})$ relation of the GFET around the neutrality point by using a parabolic function: $I = a_0(V_{ref} - V_{NP})^2 + b_0$, with a_0 and b_0 denoting the two fitting parameters. If we configure the Ag/AgCl reference electrode with a dc gate voltage close to V_{NP} = −6 mV modulated with a single-tone sinusoidal voltage $V_{ac} = A_{ac}\sin(2\pi ft)$ (sinusoidal wave in blue, V_{ac} in the inset of Fig. 1B), ideally, the corresponding rectified output current can be described as

$$I_{OUT} = I_{dc} - 0.5a_0A_{ac}^2 \cos 2\pi(2f)t + 2a_0A_{ac}\Delta V_{ref} \sin 2\pi ft \quad (1)$$

where $I_{dc} = b_0 + a_0\Delta V_{ref}^2 + 0.5a_0A_{ac}^2$ is the dc component of the output current, and ΔV_{ref} is the small gate voltage biased away from the neutrality point. It is clear that the output current contains both the second harmonic (at frequency $2f$) and the fundamental component (at frequency f), as illustrated by the gray ($I_{OUT}@2f$) and the blue ($I_{OUT}@f$) sinusoidal waves in the inset of Fig. 1B, respectively. The output at frequency $2f$ is a constant signal once the amplitude of the input sine-wave A_{ac} is fixed. In this way, one can realize a frequency-doubling device with just a single graphene transistor that gives a high-purity output spectrum (more than 90% of the total output energy) without any additional filtering, as already confirmed by our previous study (*7*). However, in contrast to previous work, here we concentrate on the output signal at frequency f, the magnitude of which is minimized (close to zero) at the neutrality point but raises proportionally to ΔV_{ref} (Eq. 1) with a prefactor $2a_0A_{ac}$. Next, we will first characterize the low-frequency noise in GFET, after which we will focus on monitoring the rectified output drain current ($I_{OUT}@f$, in response to either a step gate voltage or single-stranded DNA (ssDNA) analytes as will be shown in Figs. 3 and 4, respectively) and show that operating the GFET near its neutrality point can markedly reduce the $1/f$ noise in graphene.

In Fig. 2A, we characterized and plotted the PSD (see Materials and Methods) S_V of the GFET-I against the liquid-gate voltage V_{ref} after electrochemical cleaning. All the curves exhibit $1/f$ dependence, as indicated by the dashed gray line. We tested also the S_V at various drain-source voltage drops V_{DS} and found $S_V \propto V_{DS}^2/f$ (fig. S3), suggesting a clear $1/f$ behavior according to Hooge's empirical law (*13*). The low-frequency noise of the GFET exhibited a $1/f$ behavior, regardless of whether the measurements were performed in air or in electrolyte solution under different ionic strengths (fig. S3). In previous works, $1/f$ noise has been advantageously explored for realizing graphene-selective gas sensors (*27*, *28*). The vapors of different chemicals produce distinct effects on the low-frequency noise spectra of single pristine graphene transistors, forming unique gas signatures without specific graphene surface functionalization. This sensing mechanism also holds potential for other two-dimensional materials (*29*) and calls for future exploration.

For a more clear comparison, we plot the normalized PSD S_V/V_{DS}^2 (at $f = 10$ Hz with a bandwidth of 1 Hz) of the refreshed GFET-I as a function of the liquid-gate voltage V_{ref} in Fig. 2B (black circles). Notably, the high resistance at the neutrality point around $V_{ref} = 0.1$ V leads to a high source-drain voltage V_{DS} (in a constant-current configuration; refer also to Materials and Methods), and therefore a minimum S_V/V_{DS}^2 even if the $V_{ref} = 0.1$ V gives rise to the largest S_V (green line, Fig. 2A). After systematically investigating the $1/f$ noise behavior of graphene devices on different substrates (SiO_2, Si_3N_4, and sapphire), we conclude that the $1/f$ noise in graphene is always (local) minimum at and increases with carrier concentration around its neutrality point, revealing a "V"- or "M"-shaped feature regardless of the substrates (Fig. 2, B and C, and fig. S4), in agreement with previous reports (*13*). The typical channel area–normalized PSDs that we achieved in this study (~2×10^{-8} to 4×10^{-7} $\mu m^2/Hz$ at $f = 10$ Hz on SiO_2/Si) are comparable to the previously reported PSD level of ~10^{-8} to 10^{-7} $\mu m^2/Hz$ for micrometer-scale graphene devices on SiO_2/Si substrate (*13*). For graphene devices fabricated on Si_3N_4 substrates, we observed channel area–normalized PSDs on the order of ~1×10^{-8} $\mu m^2/Hz$ (fig. S4A) after surface refreshment, which are comparable or even superior to previously reported very low noise of suspended (~0.5×10^{-8} $\mu m^2/Hz$) (*14*) or h-BN–encapsulated (~0.5×10^{-8} to 3×10^{-8} $\mu m^2/Hz$) (*15*) graphene, making our refreshed GFETs ideal candidates for low-noise electronic biosensors.

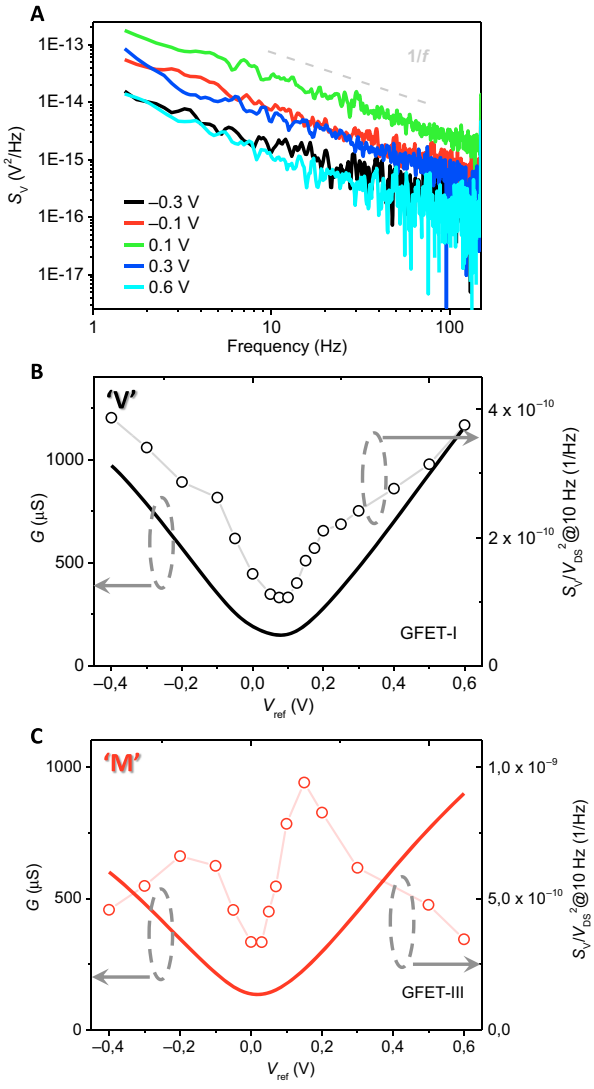

Fig. 2. 1/*f* noise performance of electrolyte-gated GFET devices. (**A**) PSD $S_V(f)$ of GFET-I at different liquid-gate voltages V_{ref} = –0.3, –0.1, 0.1, 0.3, and 0.6 V tested immediately after an initial cleaning. (**B**) $G(V_{ref})$ curves (to the left axis) and the corresponding "V"-shaped normalized PSD S_V/V_{DS}^2 (at $f = 10$ Hz with a bandwidth of 1 Hz, to the right axis) for the GFET-I after moderate electrochemical cleaning. (**C**) $G(V_{ref})$ curves (to the left axis) and the corresponding "M"-shaped normalized PSD S_V/V_{SD}^2 (at $f = 10$ Hz with a bandwidth of 1 Hz, to the right axis) for another GFET-III (also fabricated on a SiO_2/Si substrate) after moderate electrochemical cleaning.

Next, we operated the GFET near its neutrality point (Fig. 1A) and recorded the changes of the output current ΔI_f in steps of $\Delta V_{ref} = 200$ μV. At the same time, we varied the input sine-wave A_{ac} to find the most suitable value. When the amplitude of the input sine-wave A_{ac} increased from 14.1 to 70.7 mV, the sensing response (given by $\Delta I_f/200$ μV) increased linearly from 0.85 to 4.25 μS (and from 0.17 to 0.85 nA in ΔI_f; red bars, Fig. 3A). The linear behavior (dashed line in red, Fig. 3A) agrees with our proposed model ($\Delta I_f = 2a_0A_{ac}\Delta V_{ref}$; see Eq. 1). The deduced fitting parameter $a_0 = 30$ μS/V quantitatively agrees with that (29 μS/V) extracted from the parabolic fitting in Fig. 1B. As A_{ac} keeps increasing into the linear region (141.4 and 282.8 mV; gray lines, Fig. 1B), the sensing response keeps increasing but at a lower rate, because now Eq. 1 is no longer fully valid. In particular, the marked increase

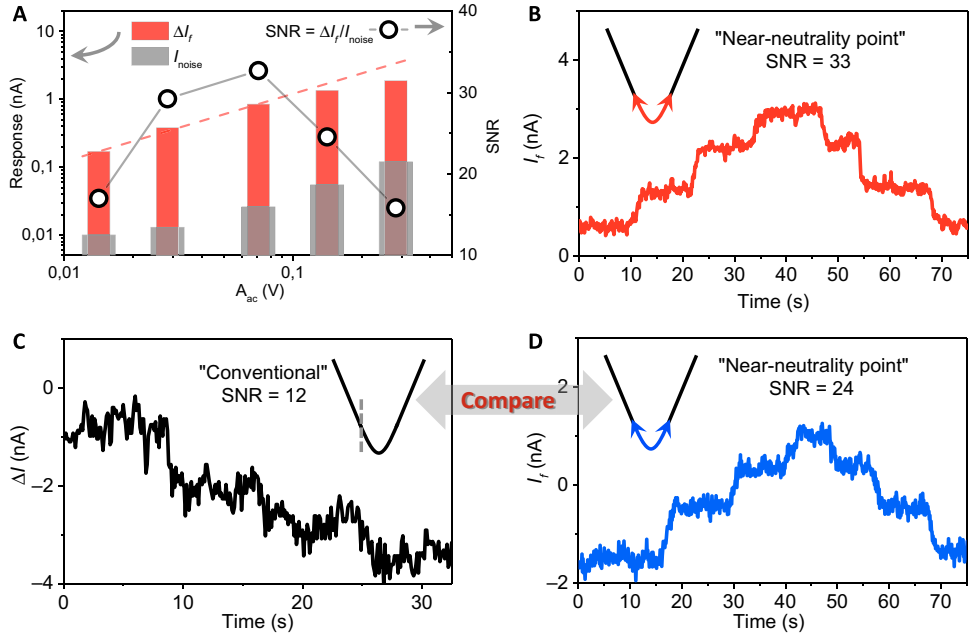

Fig. 3. Low-noise graphene transistors operated near the neutrality point. (**A**) Measured sensing response (red bars), root mean square (RMS) current noise level (gray bars), and the corresponding SNR (black circles) close to the neutrality point as a function of the amplitude A_{ac} of the gate voltage swing. The sensing current was monitored in response to a 200-μV gate voltage change after surface refreshment with a moderate electrolysis window (−0.4 V, 0.8 V). A maximum SNR of 33 was achieved at A_{in} = 70.7 mV. Its corresponding responses to a 200-μV step gate voltage change versus time is shown in (**B**). (**C** and **D**) Comparison of the GFET-II in response to the 200-μV step gate voltage change when operated in conventional mode and near the neutrality point, respectively.

in the current noise I_{noise} (measured by using a SR830 lock-in amplifier, at 1 Hz bandwidth) leads to a significantly decreased signal-to-noise ratio (SNR) = $\Delta I_f/I_{noise}$ as illustrated in Fig. 3A (black circles). It is therefore beneficial to perform the sensing test at moderate input gate voltage amplitude (A_{ac} = 70.7 mV in this case), and the corresponding response to a 200-μV step gate voltage change is shown in Fig. 3B. In Fig. 3 (C and D), we compare the actual sensing response of the GFET-II [after electrochemical cleaning at (−0.4 V, 0.6 V) but before (−0.4 V, 0.8 V)] operated in a conventional mode and in an ambipolar mode near the neutrality point, respectively. For a clear comparison, we have maintained both sensing responses at ~4 μS by adjusting the applied drain-source voltage V_{DS} (Fig. 1C) or the bias voltage V_{bias} (Fig. 1A). In the conventional mode (Fig. 3C), we operate the GFET at the outmost point of the parabolic region with an optimal SNR (section S4) and a transconductance of 4.4 μS. For the near–neutrality point operation (Fig. 3D), with A_{ac} = 70.7, we found an I_{noise} as low as 0.036 nA, which outperforms that of the conventional configuration (0.073 nA) by more than a factor of 2. This impressive enhancement of the noise performance is accompanied by an excellent sensing response of 4.25 μS, yielding an SNR of 24 in comparison to that of 12 tested in the optimized conventional configuration (Fig. 3C). We are convinced that our achievements in operating the GFET devices near the neutrality point with uncompromised sensing responses would significantly advance and extend the usage of low-noise graphene chips to a broader range of biochemical sensing applications and beyond, especially given the fact that our approaches are fully complementary to previously reported strategies for 1/*f* noise reduction (*13*–*16*). Notably, cycling the GFETs around the low-noise neutrality point can also be achieved using a back gate when exposing the devices to air (as gas sensors, for example).

Low-noise GFET biosensors

As a proof-of-principle demonstration, in this section, we apply high-performance GFET-II configured in low-noise mode near the neutrality point as potent DNA sensors. This device was cut from a 5 × 10 array of GFET devices with SU-8 liquid channel (Fig. 4A). After electrochemical cleaning, we first functionalize the surface of graphene with pyrene-linked peptide nucleic acid (pPNA) molecules 5′-AAGCTACTGGA-Lys (pyrene)-3′ (a synthetic molecule in complementary to our target HIV virus–related ssDNA molecule; see Materials and Methods). Tween 20 was then introduced to self-assemble on the graphene surface to maximize biospecific binding and ruling out possible false nonspecific positives (Fig. 4B; see also Materials and Methods) (*30*). The self-assembly process was monitored and confirmed in a conventional measurement scheme (Fig. 4C). After surface functionalization, the GFET was flushed thoroughly with an excess of 1 mM phosphate-buffered saline (PBS) buffer solution to remove unbound molecules, yielding a graphene surface with firmly adsorbed pPNA and Tween 20 molecules (as illustrated in Fig. 4B) via π-π and hydrophobic interactions.

In the next step, we investigated the chemical response of the pPNA-functionalized graphene upon ssDNA molecule adsorption in real time when operated near its neutrality point. We first injected fully complementary ssDNA molecules with a concentration of 10 pM. When the complementary ssDNA molecules reach the liquid chamber, they diffuse to the graphene channel and account for the clear sensing signal in the inset of Fig. 4D. Under an RMS SNR of 1, we can extract a limit of detection of 2 pM, which is even better than that (4 pM) of our previously reported ultrasensitive DNA sensors (*7*). To confirm the specificity of our detection, we introduced 1-base mismatched ssDNA at the same concentrations of 10 pM, and no noticeable signal was observed (fig. S6). We also injected fully complementary ssDNA molecules with a

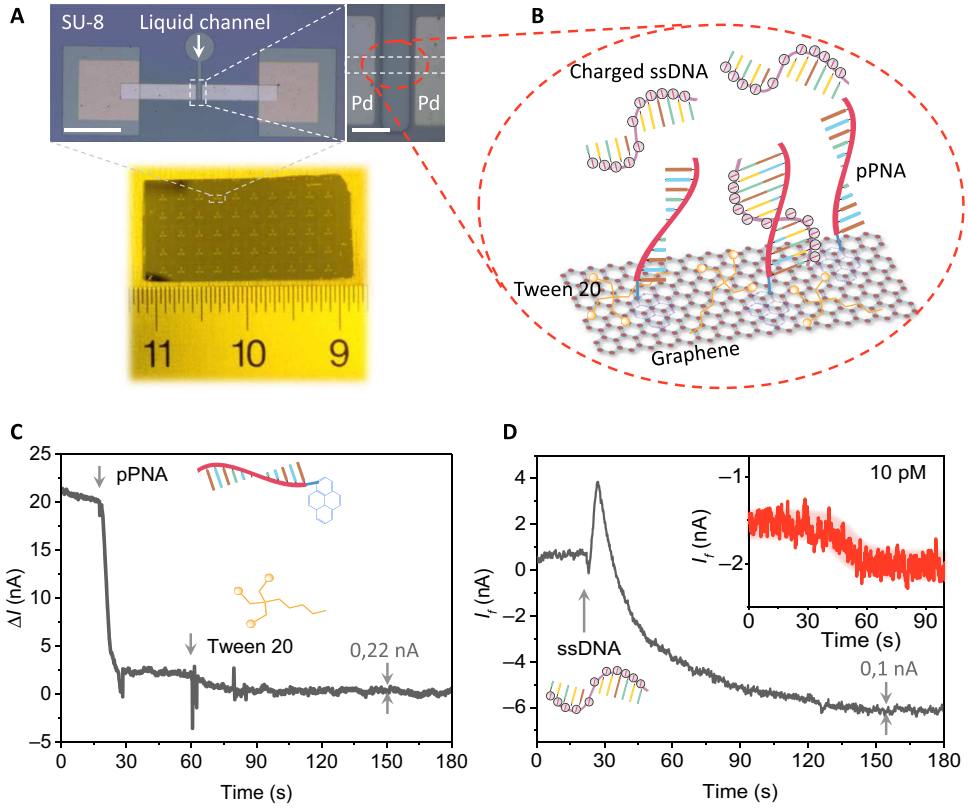

Fig. 4. DNA sensing near the neutrality point of graphene. (**A**) Upper panel: Optical micrographs of GFET-II. The left image shows the openings defined by a 1-μm-thick SU-8 photoresist. Scale bar, 200 μm. The right image is a zoom of the SU-8 liquid channel across a graphene flake (white dashed lines in between the two Pd electrodes). Scale bar, 20 μm. Lower panel: A 5 × 10 GFET device array fabricated on a SiO_2/Si substrate. (**B**) Schematic illustration of negatively charged complementary ssDNA molecules bind to pPNA molecules that are noncovalently anchored on the graphene surface. Nonspecific binding of biomolecules directly on the GFET was prevented by self-assembling Tween 20 on the graphene surface. (**C**) Changes in Δ*I* of the graphene sensor in a conventional GFET measurement scheme upon the self-assembly processes of pPNA and Tween 20 with concentrations of 1 μM and 0.05 wt %, respectively. Current noise, 0.22 nA. (**D**) Changes in I_f of the graphene sensor operated near its neutrality point versus time upon the introduction of 1 nM and 10 pM (inset) fully complementary ssDNA. Current noise, 0.1 nA. All were tested in 1 mM PBS buffer solution.

concentration of 1 nM (as indicated by the initial spike upon ssDNA solution injection, which suggests a rapid response of the sensor). Its magnitude is 7 nA, sitting on a background noise of 0.1 nA, confirming our observed positive signal at 10 pM ssDNA. It is also clear that by cycling the ambipolar graphene transistor around its neutrality point, the current noise in Fig. 4D (0.1 nA) is significantly reduced compared to that (0.22 nA) in Fig. 4C operated in a conventional GFET measurement scheme (with similar sensing responses).

It is noteworthy that all our experiments are based on single-layer graphene (fig. S1; see also Materials and Methods). The 1/*f* noise in graphene depends on the number of layers. Double- or few-layer graphene devices are expected to reduce the 1/*f* noise (*16*, *31*). We believe that the optimization of graphene biosensors calls for additional studies of the number of layers on both the 1/*f* noise level and the sensing response in liquid environments. This is because the band structure and electrical properties of few-layer graphene are different from those of single-layer graphene. Few-layer graphene devices would lose the steep I-V_{GS} curve observed for single-layer graphene (*31*), leading to significant reduction in the GFET amplification and degradation in the sensing response. In this regard, single-layer graphene with a large sensing response (as investigated in the current work) is likely optimal for graphene sensor application, as also advocated in the literature reporting single-layer graphene-based biosensors with superior performance (*4*, *11*, *12*). Nevertheless, the techniques that we proposed in this article deal with the reduction of 1/*f* noise, which is dominated by surface over bulk noise in graphene up to seven layers (*31*). Thus, our noise reduction techniques for graphene sensor applications near the neutrality point also hold potential for few-layer devices.

CONCLUSION

We demonstrate that operating a graphene transistor in an ambipolar mode near its neutrality point can markedly reduce the 1/*f* noise in graphene. The development of low-noise, portable, and reliable graphene sensors for point-of-care applications is at the frontier of graphene electronics and biosensors and could have an enormous societal impact for the broader field of medical diagnosis. Along with the electrochemical surface refreshment technology introduced in this paper, we expect that our crucial improvements in device sensitivity and reliability of graphene electronics operated in a liquid environment will be important in this pursuit, as well as for new insights into the 1/*f* noise mechanisms in graphene.

MATERIALS AND METHODS

CVD graphene growth and transfer

Single-crystal monolayer graphene films (fig. S1) were grown by CVD using a gas mixture of Ar, H_2, and diluted CH_4 [200 parts per million

(ppm) CH_4 balanced in argon] on 25-μm-thick copper foils (99.8%, Alfa Aesar, 13382). After washed by acetone and HCl/H_2O (1:20), the copper foils were thoroughly rinsed in deionized (DI) water and blow-dried (N_2). The cleaned copper foils were then loaded into a homebuilt CVD system and preannealed at 1050°C under a flow of 100-sccm (standard cubic centimeter per minute) Ar at 0.8 bar for 2 hours. Thereafter, single-crystal graphene was grown at 1050°C and 10 torr for 5 hours under a flow of 100-sccm Ar, 10-sccm hydrogen, and 20-sccm diluted CH_4. The growth was terminated by quenching the quartz tube in ambient environment (cooling rate, ~100°C/min).

The transfer of the CVD graphene films on the copper foils was carried out by first spin-coating a poly(methyl 2-methylpropenoate) (PMMA) film over the graphene film. After etching away the graphene coverage on the other side by O_2 plasma, the copper films were dissolved in an ammonium persulfate solution. The solution was exchanged with DI water for several times before the graphene/PMMA films were transferred onto various substrates. Eventually, the PMMA films could be dissolved using acetone, leaving uniform, large-area monolayer graphene on the substrate for further processing.

Device fabrication

The preparation of GFET devices on sapphire can be found elsewhere (*4*). The rest of the electrolyte-gated GFET devices were fabricated either on undoped Si substrates with ~100-nm dry SiO_2 or on undoped SiO_2/Si substrates with 100-nm plasma-enhanced CVD low-stress Si_3N_4. Both substrates were precoated with HMDS (*19*). These electrolyte-gated GFET devices were patterned and metalized (60-nm Pd) by using standard electron-beam lithography technique, resulting in transistors having a length of 20 μm and a width of 10 μm on a SiO_2/Si substrate and 10 μm by 10 μm on a Si_3N_4/SiO_2/Si substrate. As schematically sketched in Fig. 1 (A and C), the liquid handling was achieved via a sequential fabrication of (i) a PMMA or SU-8 layer to define the micrometer-sized liquid channel and after wire bonding and (ii) a biocompatible, two-component epoxy to seal the contact. Before electrical characterization, all the devices were baked (200°C) for at least 1 hour under vacuum or ambient conditions and thoroughly rinsed in isopropanol.

Electrostatic-assisted electrochemical refreshment of graphene surface

A mild cyclic liquid-gate voltage applied to a GFET can very rapidly remove its surface contaminants—introduced during either CVD graphene transfer or device fabrication/storage (see section S2). Here, a conservative electrochemical condition of (−0.4 V, 0.6 V) and a moderate condition of (−0.4 V, 0.8 V) were applied for Figs. 1D and 2 (C and D), respectively, at a sweeping rate of ~1 to 10 mV/s against an Ag/AgCl reference electrode when the graphene conductive channel was held at ground. As schemed in fig. S2, to further accelerate the electrochemical processes, a sine wave with V_{in} = 70.7 mV with relatively high frequency (77.77 Hz) was superpositioned on the liquid gate. The oscillatory voltage imposed a periodic force on charged nanoparticles and impurities on or close to the graphene surface. Loosely adsorbed nanoparticles and impurities spread out and diffused away into the bulk of the buffer solution. In addition, the oscillatory voltage was promised to speed up the electrolytic reactions, and thus allowing an improved outcome, through facilitating and accelerating the diffusion of reactive agents. Notably, we expect that the electrochemical cleaning technique can be adopted to clean the surface of back-gated GFETs if followed by thorough rinsing and blow-drying.

Noise characterizations

For electronic noise characterization in general, a clean current source I_{DS} (homemade battery-based) was connected to the drain electrode, and the corresponding voltage drop over the graphene channel V_{DS} was monitored and analyzed by using a dynamic signal analyzer (HP35670a; see fig. S3A). In Fig. 3 (B to D), the background electronic noise was tested by using an SR830 lock-in amplifier (Stanford Research Systems). In Fig. 4 (C and D), the background noise was estimated from the SD of the data sets.

Noncovalent surface functionalization of graphene

The PNA molecules 5′-AAGCTACTGGA-Lys (pyrene)-3′ is a synthetic molecule complementary to our target HIV virus–related ssDNA molecule (*32*) 5′-TCCAGTAGCTT-3′ and its 1-base mismatched molecule 5’-TCCAGAAGCTT-3′ (all purchased from Eurogentec S.A.). In Fig. 3B, Lys (pyrene) is a molecular linker group with a pyrene unit, which can be noncovalently anchored onto graphene surface via π-π interaction. To prevent nonspecific binding of biomolecules directly to the GFET, Tween 20 was then applied to self-assemble on the graphene surface in 1 mM PBS solution with 0.05 weight % (wt %) concentration. Tween 20 owns two important parts: an aliphatic chain that can immobilize on the hydrophobic graphene surface by noncovalent interaction, and aliphatic ester chains that can prevent nonspecific binding of biomolecules, thus maximizing biospecific binding to the surface-anchored recognition probes and ruling out possible false positives (*30*). We note here that the noise level of the device had a tendency to increase after the surface functionalization. We ascribe the slight increase in the electrical noise to the unbinding/free sites of the surface PNA molecules, which could, in principle, introduce trap states and current fluctuations, in accordance with previous reports (*33*).

SUPPLEMENTARY MATERIALS

Supplementary material for this article is available at http://advances.sciencemag.org/cgi/content/full/3/10/e1701247/DC1

section S1. Single-crystal monolayer CVD graphene
section S2. Electrochemical cleaning of graphene: Basic principle
section S3. Noise characterizations
section S4. SNR in conventional operated GFETs
section S5. pPNA-DNA hybridization: 1-base mismatched
fig. S1. High-quality single-crystal CVD graphene.
fig. S2. Schematic presentation of in situ electrochemical cleaning of an electrolyte-gated GFET device.
fig. S3. Electronic noise characterization for graphene on SiO_2/Si substrate.
fig. S4. Electronic noise characterization for graphene on Si_3N_4/Si and sapphire substrates.
fig. S5. SNR in conventional operated GFET devices.
fig. S6. No obvious changes in I_f of the graphene biosensor versus time upon the introduction of 10 pM 1-base–mismatched ssDNA in 1 mM PBS solution.
References (*34*–*36*)

REFERENCES AND NOTES

1. P. Bergveld, Thirty years of ISFETOLOGY: What happened in the past 30 years and what may happen in the next 30 years. *Sens. Actuators B* **88**, 1–20 (2003).
2. P. Bergveld, Development of an ion-sensitive solid-state device for neurophysiological measurements. *IEEE Trans. Biomed. Eng.* **17**, 70–71 (1970).
3. Y. Ohno, K. Maehashi, Y. Yamashiro, K. Matsumoto, Electrolyte-gated graphene field-effect transistors for detecting pH protein adsorption. *Nano Lett.* **9**, 3318–3322 (2009).
4. L. H. Hess, M. Jansen, V. Maybeck, M. V. Hauf, M. Seifert, M. Stutzmann, I. D. Sharp, A. Offenhäusser, J. A. Garrido, Graphene transistor arrays for recording action potentials from electrogenic cells. *Adv. Mater.* **23**, 5045–5049 (2011).
5. A. Fabbro, D. Scaini, V. León, E. Vázquez, G. Cellot, G. Privitera, L. Lombardi, F. Torrisi, F. Tomarchio, F. Bonaccorso, S. Bosi, A. C. Ferrari, L. Ballerini, M. Prato, Graphene-based interfaces do not alter target nerve cells. *ACS Nano* **10**, 615–623 (2016).

6. S. J. Heerema, C. Dekker, Graphene nanodevices for DNA sequencing. *Nat. Nanotechnol.* **11**, 127–136 (2016).
7. W. Fu, L. Feng, D. Mayer, G. Panaitov, D. Kireev, A. Offenhäusser, H.-J. Krause, Electrolyte-gated graphene ambipolar frequency multipliers for biochemical sensing. *Nano Lett.* **16**, 2295–2300 (2016).
8. C. Mackin, T. Palacios, Large-scale sensor systems based on graphene electrolyte-gated field-effect transistors. *Analyst* **141**, 2704–2711 (2016).
9. D. Sarkar, W. Liu, X. Xie, A. C. Anselmo, S. Mitragotri, K. Banerjee, MoS_2 field-effect transistor for next-generation label-free biosensors. *ACS Nano* **8**, 3992–4003 (2014).
10. N. C. S. Vieira, J. Borme, G. Machado, F. Cerqueira, P. P. Freitas, V. Zucolotto, N. M. R. Peres, P. Alpuim, Graphene field-effect transistor array with integrated electrolytic gates scaled to 200 mm. *J. Phys. Condens. Mat.* **28**, 085302 (2016).
11. W. Fu, L. Jiang, E. P. van Geest, L. M. C. Lima, G. F. Schneider, Sensing at the surface of graphene field-effect transistors. *Adv. Mater.* **29**, 1603610 (2017).
12. G. Xu, J. Abbott, L. Qin, K. Y. M. Yeung, Y. Song, H. Yoon, J. Kong, D. Ham, Electrophoretic and field-effect graphene for all-electrical DNA array technology. *Nat. Commun.* **5**, 4866 (2014).
13. A. A. Balandin, Low-frequency 1/*f* noise in graphene devices. *Nat. Nanotechnol.* **8**, 549–555 (2013).
14. Z. Cheng, Q. Li, Z. Li, Q. Zhou, Y. Fang, Suspended graphene sensors with improved signal and reduced noise. *Nano. Lett.* **10**, 1864–1868 (2010).
15. M. A. Stolyarov, G. Liu, S. L. Rumyantsev, M. Shur, A. A. Balandin, Suppression of 1/*f* noise in near-ballistic *h*-BN-graphene-*h*-BN heterostructure field-effect transistors. *Appl. Phys. Lett.* **107**, 023106 (2015).
16. Y. M. Lin, P. Avouris, Strong suppression of electrical noise in bilayer graphene nanodevices. *Nano Lett.* **8**, 2119–2125 (2008).
17. F. Schedin, A. K. Geim, S. V. Morozov, E. W. Hill, P. Blake, M. I. Katsnelson, K. S. Novoselov, Detection of individual gas molecules adsorbed on graphene. *Nat. Mater.* **6**, 652–655 (2007).
18. C.-T. Lin, P. T. K. Loan, T.-Y. Chen, K.-K. Liu, C.-H. Chen, K.-H. Wei, L.-J. Li, Label-free electrical detection of DNA hybridization on graphene using hall effect measurements: Revisiting the sensing mechanism. *Adv. Funct. Mater.* **23**, 2301–2307 (2013).
19. M. Lafkioti, B. Krauss, T. Lohmann, U. Zschieschang, H. Klauk, K. v. Klitzing, J. H. Smet, Graphene on a hydrophobic substrate: Doping reduction and hysteresis suppression under ambient conditions. *Nano Lett.* **10**, 1149–1153 (2010).
20. D. Y. Jung, S. Y. Yang, H. Park, W. C. Shin, J. G. Oh, B. J. Cho, S.-Y. Choi, Interface engineering for high performance graphene electronic devices. *Nano Converg.* **2**, 11 (2015).
21. S. Raghavan, C. C. Chiang, Review—Understanding and controlling electrochemical effects in wet processing. *ECS J. Solid State Sci. Technol.* **5**, P309–P314 (2016).
22. X. W. Yang, H. L. Peng, Q. Xie, Y. Zhou, Z. F. Liu, Clean and efficient transfer of CVD-grown graphene by electrochemical etching of metal substrate. *J. Electroanal. Chem.* **688**, 243–248 (2013).
23. H.-T. Fang, C.-G. Liu, C. Liu, F. Li, M. Liu, H.-M. Cheng, Purification of single-wall carbon nanotubes by electrochemical oxidation. *Chem. Mater.* **16**, 5744–5750 (2004).
24. M. H. Schoenfisch, A. M. Ross, J. E. Pemberton, Electrochemical cleaning of surface-confined carbon contamination in self-assembled monolayers on polycrystalline Ag and Au. *Langmuir* **16**, 2907–2914 (2000).
25. S. Das Sarma, S. Adam, E. H. Hwang, E. Rossi, Electronic transport in two-dimensional graphene. *Rev. Mod. Phys.* **83**, 407–470 (2011).
26. H. Wang, D. Nezich, J. Kong, T. Palacios, Graphene frequency multipliers. *IEEE Electr. Device L* **30**, 547–549 (2009).
27. S. Rumyantsev, G. Liu, M. S. Shur, R. A. Potyrailo, A. A. Balandin, Selective gas sensing with a single pristine graphene transistor. *Nano Lett.* **12**, 2294–2298 (2012).
28. S. Rumyantsev, G. Liu, R. A. Potyrailo, A. A. Balandin, M. S. Shur, Selective sensing of individual gases using graphene devices. *IEEE Sens. J.* **13**, 2818–2822 (2013).
29. G. Liu, S. L. Rumyantsev, C. Jiang, M. S. Shur, A. A. Balandin, Selective gas sensing with *h*-BN capped MoS_2 heterostructure thin-film transistors. *IEEE Electr. Device L* **36**, 1202–1204 (2015).
30. L. Feng, L. Wu, J. Wang, J. Ren, D. Miyoshi, N. Sugimoto, X. Qu, Detection of a prognostic indicator in early-stage cancer using functionalized graphene-based peptide sensors. *Adv. Mater.* **24**, 125–131 (2012).
31. G. Liu, S. Rumyantsev, M. S. Shur, A. A. Balandin, Origin of 1/*f* noise in graphene multilayers: Surface vs. volume. *Appl. Phys. Lett.* **102**, 093111 (2013).
32. H. Kuhn, V. V. Demidov, J. M. Coull, M. J. Fiandaca, B. D. Gildea, M. D. Frank-Kamenetskii, Hybridization of DNA and PNA Molecular Beacons to Single-Stranded and Double-Stranded DNA Targets. *J. Am. Chem. Soc.* **124**, 1097–1103 (2002).
33. S. Sorgenfrei, C.-Y. Chiu, M. Johnston, C. Nuckolls, K. L. Shepard, Debye screening in single-molecule carbon nanotube field-effect sensors. *Nano Lett.* **11**, 3739–3743 (2011).
34. A. Ambrosi, M. Pumera, The CVD graphene transfer procedure introduces metallic impurities which alter the graphene electrochemical properties. *Nanoscale* **6**, 472–476 (2014).
35. Y.-C. Lin, C.-C. Lu, C.-H. Yeh, C. Jin, K. Suenaga, P.-W. Chiu, Graphene annealing: How clean can it be? *Nano Lett.* **12**, 414–419 (2012).
36. Y. Su, H.-L. Han, Q. Cai, Q. Wu, M. Xie, D. Chen, B. Geng, Y. Zhang, F. Wang, Y. R. Shen, C. Tian, Polymer adsorption on graphite and CVD graphene surfaces studied by surface-specific vibrational spectroscopy. *Nano Lett.* **15**, 6501–6505 (2015).

Acknowledgments: We thank C. Schönenberger and Y. Zhang for helpful discussions. **Funding:** The research leading to this article has gratefully received funding from the Alexander von Humboldt Foundation, the Netherlands Organisation for Scientific Research (722.014.004), the Swiss National Science Foundation (P300P2_154557), the Shanghai Institutions of Higher Learning (no. TP2016023), and the National Natural Science Foundation of China (21705106). **Author contributions:** W.F., H.-J.K., and A.O. designed the experiments. W.F. fabricated the GFET devices and performed the experiments. L.F. and D.M. conceived and performed the pPNA-DNA hybridization experiment with W.F. D.K. contributed to the noise test of the GFET devices fabricated on a sapphire substrate. W.F., G.P., and H.-J.K. wrote the manuscript. All the authors read and commented on the manuscript. **Competing interests:** The authors declare that they have no competing interests. **Data and materials availability:** All data needed to evaluate the conclusions in the paper are present in the paper and/or the Supplementary Materials. Additional data related to this paper may be requested from the authors.

Submitted 19 April 2017
Accepted 26 September 2017
Published 25 October 2017
10.1126/sciadv.1701247

Citation: W. Fu, L. Feng, G. Panaitov, D. Kireev, D. Mayer, A. Offenhäusser, H.-J. Krause, Biosensing near the neutrality point of graphene. *Sci. Adv.* **3**, e1701247 (2017).

Biosensing near the neutrality point of graphene

Wangyang Fu, Lingyan Feng, Gregory Panaitov, Dmitry Kireev, Dirk Mayer, Andreas Offenhäusser and Hans-Joachim Krause

Sci Adv **3** (10), e1701247.
DOI: 10.1126/sciadv.1701247